

# An Earthworm-Inspired Soft Crawling Robot Controlled by Friction

Joey Z. Ge, Ariel A. Calderón, and Néstor O. Pérez-Arancibia

**Abstract**— We present the modeling, design, fabrication and feedback control of an earthworm-inspired soft robot capable of crawling on surfaces by actively manipulating the frictional force between its body and the surface. Earthworms are segmented worms composed of repeating units known as metameres. The muscle and setae structure embedded in each individual metamere makes possible its peristaltic locomotion both under and above ground. Here, we propose a pneumatically-driven soft robotic system made of parts analogous to the muscle and setae structure and can replicate the crawling motion of a single earthworm metamere. A model is also introduced to describe the crawling dynamics of the proposed robotic system and proven be controllable. Robust crawling locomotion is then experimentally verified.

## I. INTRODUCTION

Animal locomotion has long been a source of inspiration for robotic research. Limbless locomotion has been gaining attention as at times it can be the superior method of traveling on marginal terrains. Earthworms are possibly one of the most familiar animals that travel in a limbless gait. Some of the earthworm species are commonly known as the ‘night crawlers’ due to the fact that they remain underground during the day and crawl above ground at night. These earthworms have evolved to adapt to different surroundings, developing robust and highly adaptable locomotive mechanisms that enable them to maneuver through their labyrinthine underground burrows and crawl over complex terrains. Specifically, earthworms travel by peristalsis, a motion achieved by repeated successive contraction and relaxation of its longitudinal and circular muscles embedded in each body segment. Such periodic motion travels posteriorly along the body, generating the retrograde peristaltic wave that propels the body forward [1]–[3]. In addition, bristle-like structures called setae are employed to manipulate traction [4], [5].

Versatility, robustness and spatial efficiency make earthworms’ peristaltic gait a very attractive case for robotic locomotion development. Numerous studies have focused on creating robots that can replicate earthworms’ peristalsis, adopting a variety of different actuation technologies including *shape memory alloys* (SMAs) [6]–[8], magnetic fluids [9] and electric motors [10]–[12]. Recent progress in innovative fabrication methods have made possible the development of biologically-inspired soft actuators, soft sensors and flexible electronics [13]–[15]. An earthworm-inspired burrowing robot that incorporates these technologies is presented in

This work was partially supported by the USC Viterbi School of Engineering through fellowships to J. Z. Ge, and A. A. Calderón and a start-up fund to N. O. Pérez-Arancibia, and partially by the Chilean National Office of Scientific and Technology Research (CONICYT) through a graduate fellowship to A. A. Calderón.

J. Z. Ge, A. A. Calderón, and N. O. Pérez-Arancibia are with the Department of Aerospace and Mechanical Engineering, University of Southern California (USC), Los Angeles, CA 90089-1453, USA (e-mail: zaoyuang@usc.edu, aacalder@usc.edu, and perezara@usc.edu).

[16]. However, such robot’s locomotion is contingent upon being fully enclosed in a tube of certain sizes and the surface crawling capability of earthworm is yet to be addressed.

In this work, we introduce an earthworm-inspired soft robot that is capable of generating peristaltic crawling on surface by actively manipulating frictional force between its body and ground. Friction is a major factor in terrestrial locomotion. Drawing inspiration from nature, studies have developed different methods to exploit frictional forces, including gecko-like friction adhesive [17], microspine [18], [19] and anisotropic friction mechanisms [20], [21]. [22] presents a robot that employs materials of different coefficients of friction as well as a pair of unidirectional clutches to manipulate the frictional force in order to generate locomotion. The soft robot proposed here is composed of two types of pneumatically driven soft actuators that emulate the functions of earthworms’ longitudinal and circular muscles. A pair of hard casings are also integrated into the design to create a friction differential that enables locomotion. In addition, we model the dynamics of the robot as a *linear time invariant* (LTI) system and prove that the frictional force can well be employed as the input signal making the system controllable.

The rest of the paper is organized as follows. Section II introduces some major concepts unique to earthworm-inspired locomotion. Section III presents the dynamic modeling as well as the simulated locomotion results of the earthworm-inspired robot. Section IV explains design and fabrication process of the proposed robot. Section V describes the locomotion planning and associated control strategy. Experimental results are demonstrated and discussed in Section VI. Lastly, Section VII concludes the paper and provides outlook for future research.

## II. EARTHWORM INSPIRED LOCOMOTION

Earthworms belong to the phylum *annelida*, distinguished by their segmented body structure. The ring-shaped segment is known as metamere, shown in Fig. 1-(a). Each metamere is surrounded by a layer of longitudinal muscle on top of which lays another layer of circular muscle. The body cavity (coelom) of earthworm is filled with incompressible coelomic fluid which acts as an internal hydrostatic skeleton. Furthermore, coelomic fluid is constrained within each segment partitioned by septa so there is no movement of the fluid across each metamere [3]. Such segmentation preserves, to some extent, the locomotion independence of each metamere, enhancing earthworms’ overall mobility [1]. To advance, the longitudinal and circular muscle of each segment contract alternately under constant volume, causing each segment to shorten (radially expanding) and elongate (radially shrinking). All the segments successively repeat such motion from head to tail, forming the retrograde peristaltic gait. Moreover,

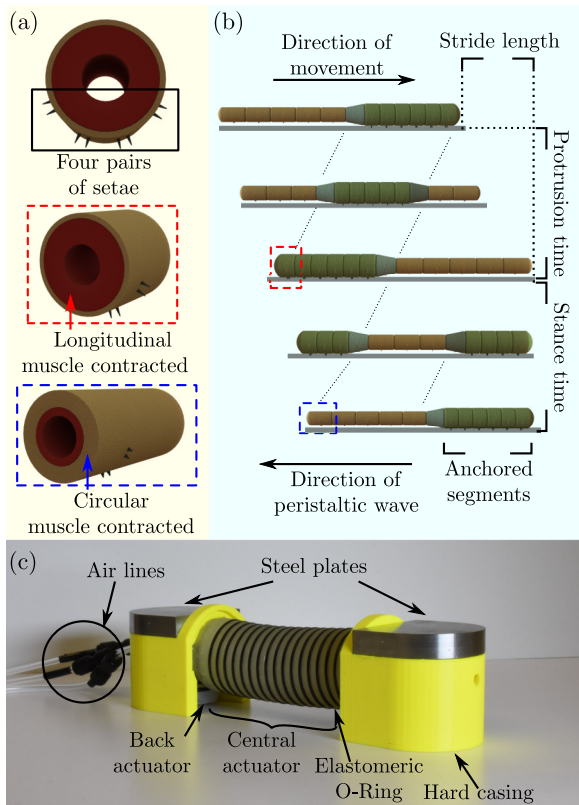


Fig. 1. (a) **Metamere**: Four pairs of setae are distributed on the lateral and ventral surface of each metamere. Each metamere expands radially and contracts longitudinally at the same time when the longitudinal muscle contracts and the circular muscle relaxes, and vice versa. (b) **Peristaltic crawling motion**: When crawling, setae will protrude from radially expanded segments therefore provide anchoring. One stride is defined as a complete cycle of peristalsis and stride length is the total length advanced during one stride. The protrusion time is characterized as the time duration during which earthworm moves forward. The head of the earthworm will have covered the stride length by the end of protrusion time. Correspondingly, stance time is the period during which the head of earthworm remains anchored to the ground while the rest of earthworm body recovers to the initial condition. The sum of the protrusion time and stance time is the stride period. The dotted lines address the retrograde wave observed in peristalsis. (c) **Earthworm-inspired crawling robot**: The robot consists of two hard casings, a central actuator and a pair of front and rear actuators bound by elastomeric o-rings, two machined steel plates and pneumatic components.

each metamere of an earthworm bears setae, a feature found in *oligochaetas*, a sub-group of *annelida*. Some species of earthworm are both geophagous (earth-eaters) and surface-feeders [4]. Commonly known as ‘night crawlers’, these earthworms emerge from their burrows and crawl on ground at night and remain underground during daytime [23]. To adapt to the two different surroundings, they switch between crawling and burrowing to generate locomotion accordingly. Both gaits use peristalsis but we focus on the crawling motion in this study. From a morphological point of view, these ‘night crawlers’ have evolved to bear setae only on the ventral and lateral surface of each segment illustrated in Fig. 1-(a) to facilitate surface crawling, as opposed to purely geophagous earthworms, of which setae are arranged in a ring around each segment [3], [5]. When crawling, setae will protrude from segments undergoing radial expansion (longitudinal muscle contraction) and anchor into the substratum to provide traction that can prevent these segments from slipping when circular muscles of adjacent metameres

contract. Once the circular muscle starts to relax, the setae will retract from the ground to allow the segment to move forward.

We design the crawling gait of our proposed robot based on locomotion the mechanism depicted in Fig. 1-(b). Following [4], we define a *stride* as one cycle of peristalsis and we describe the crawling kinematics as a function of four variables: *stride length*, *protrusion time*, *stance time* and *stride period*. Notice that earthworms have numerous segments with staggered stride periods, so for the purpose of simplicity, all four variables introduced here are chosen to describe earthworms’ very first segment. Fig. 1-(c) presents the earthworm-inspired crawling robot we develop in this work. It is composed of pneumatic soft actuators emulating earthworms’ muscle structure as well as hard casings that can regulate friction. This robot is more analogous to a single metamere of an earthworm than to a worm as a whole. The modeling and development process is discussed in the following sections.

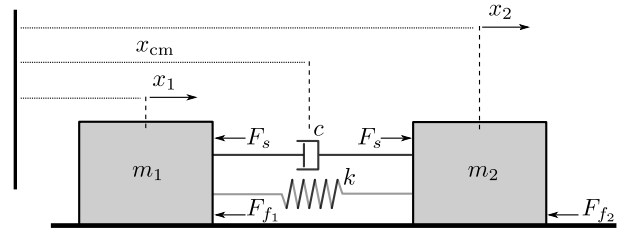


Fig. 2. Mass-spring model of the robot presented in this paper. The controllability analysis was carried out for two cases: without friction and with frictions  $F_{f1}$  and  $F_{f2}$  included as input.

### III. MODEL SIMULATION AND RESULTS

#### A. Dynamics modeling and controllability analysis

Several of the existing earthworm-inspired robots consist of three segments, a pair of posterior and anterior parts that serve as the artificial circular muscle and an axial central actuator which is comparable to the earthworm’s longitudinal muscle [8], [16], [24]. Limited by their configurations, these robots can only travel within pipes. During locomotion, they replicate the peristaltic burrowing locomotion of earthworms as their anterior and posterior actuators alternately provide anchoring while the longitudinal actuator extends and contracts to generate displacement. Given its function and elastic characteristics, the longitudinal actuator can be modeled as a massless elastic spring with stiffness constant of  $k$ . The anterior and posterior segments can be approximated as two blocks of masses  $m_1$  and  $m_2$ . Therefore, if taken out of the pipe and enabled to crawl on ground, this type of robots shares similar dynamics to the mass-spring system shown in Fig. 2. For a pneumatically actuated soft robot [16], the equivalent spring force  $F_s$  is realized by internal gauge pressure translated to the two ends of longitudinal actuator; and according to *Hooke’s Law*, is equivalent to the product of the spring stiffness and the deformation length

$$F_s = k\Delta l = P_{\text{long}}S, \quad (1)$$

where  $\Delta l$  is the deformation of the spring,  $P_{\text{long}}$  is the internal gauge pressure, and  $S$  is the cross-sectional area of the longitudinal actuator. Notice that we approximate

the stiffness  $k$  to be a constant in our model, however the longitudinal actuator is not massless and  $k$  is very likely to vary with the actuator internal pressure. Therefore, quantitatively finding such relation and refining the model are objectives of future research. A damping coefficient  $c$  is also introduced in the system to address natural energy dissipation, shown as the damper in Fig. 2.

We first demonstrate that the system is uncontrollable if we assume that there is no friction between contacting surfaces. Under this assumption, if we choose the equivalent spring force  $F_s$  to be the sole input and let the positions as well as the velocities to be the output, we can quickly arrive at the state-space realization of this *single-input multi-output* (SIMO) LTI system as follows if we define the state  $x$  to be the displacements of two masses,  $x_1, x_2$ , as well as their velocities,  $v_1 = \dot{x}_1$  and  $v_2 = \dot{x}_2$ , respectively,

$$\begin{aligned} \dot{x}(t) &= Ax(t) + Bu(t) \\ y(t) &= Cx(t) + Du(t) \end{aligned} \quad (2)$$

$$A = \begin{bmatrix} 0 & 1 & 0 & 0 \\ -\frac{k}{m_1} & -\frac{c}{m_1} & \frac{k}{m_1} & \frac{c}{m_2} \\ 0 & 0 & 0 & 1 \\ \frac{k}{m_2} & \frac{c}{m_2} & -\frac{k}{m_2} & -\frac{c}{m_2} \end{bmatrix}, B = \begin{bmatrix} 0 \\ -\frac{1}{m_1} \\ 0 \\ \frac{1}{m_2} \end{bmatrix} \quad (3)$$

$$C = \begin{bmatrix} 1 & 0 & 0 & 0 \\ 0 & 1 & 0 & 0 \\ 0 & 0 & 1 & 0 \\ 0 & 0 & 0 & 1 \end{bmatrix}, D = \begin{bmatrix} 0 \\ 0 \\ 0 \\ 0 \end{bmatrix}.$$

However, the corresponding controllability matrix

$$C = [B \quad AB \quad A^2B \quad A^3B] \quad (4)$$

has rank of 2 instead of full row rank 4, thus the system is not controllable, meaning that there does not necessarily exist an input sequence that can transfer the robot itself from any given initial position and velocity set to any final location at certain velocity within a finite time period [25]. Associated with the controllability matrix is the controllable subspace  $\mathcal{C}_{AB}$ , which is defined as the range space or the image of the controllability matrix [26]. Such subspace is spanned by all possible linear combinations of all the linearly independent columns of the controllability matrix, known as the basis of the controllability subspace. In our case,  $\mathcal{C}_{AB}$  is spanned with

$$\left\{ \alpha_1 \begin{pmatrix} 1 \\ 0 \\ -\frac{m_1}{m_2} \\ 0 \end{pmatrix}, \alpha_2 \begin{pmatrix} 0 \\ 1 \\ 0 \\ -\frac{m_1}{m_2} \end{pmatrix} \right\} \quad (5)$$

where  $\alpha_1, \alpha_2 \in \mathbb{R}$ . According to [26], the set of reachable states  $\mathcal{R}_t$  of a system at any time greater than 0 is equivalent to  $\mathcal{C}_{AB}$ . The reachable positions for the masses take the form of  $x_1 = \alpha_1$  and  $x_2 = -\alpha_1 \frac{m_1}{m_2}$ . Then clearly, the position of center of mass of this system  $x_{cm}$ , defined as

$$x_{cm} = \frac{m_1 x_1 + m_2 x_2}{m_1 + m_2}, \quad (6)$$

is always 0. This indicates that no input will cast any influence on the system as a whole, further validating that the full system is uncontrollable.

In the following, we prove that we can attain system controllability by incorporating frictional force as control input to the system. Such finding provides us valuable insight into design of both the physical trait as well as control algorithm for the crawling robot.

As shown in Fig. 2,  $F_{f_1}$  and  $F_{f_2}$  represent the frictional force between the two mass blocks and the ground. Frictional force has been the research interest of many fields and various friction modeling procedures have evolved with foci on different interfaces, parameter dependences and classes of contact [27]. Considering the slow speed of earthworms as well as our model setup, we assume  $F_{f_1}$  and  $F_{f_2}$  to be basic kinetic friction that takes the form of the product between coefficient of kinetic friction and normal force.  $F_{f_1}$  and  $F_{f_2}$  are of opposite directions to the velocities of the two mass blocks,  $v_1$  and  $v_2$ , respectively. Therefore, the new input  $u^*(t)$  to the system has three entries,

$$u^*(t) = [F_s \quad F_{f_1} \quad F_{f_2}]^T(t). \quad (7)$$

Matrices  $A, C$  and  $D$  remain unchanged while the new  $B$  matrix, denoted as  $B^*$  takes on the following form

$$B^* = \begin{bmatrix} 0 & 0 & 0 \\ -\frac{1}{m_1} & -\frac{1}{m_1} & 0 \\ 0 & 0 & 0 \\ \frac{1}{m_2} & 0 & -\frac{1}{m_2} \end{bmatrix}. \quad (8)$$

This now *multi-input multi-output* (MIMO) system has a new controllability matrix  $C^* \in \mathbb{R}^{4 \times 12}$ , and it has full row rank. Thus the system is proven to be controllable. Furthermore, the new controllability subspace  $\mathcal{C}_{AB}$  is spanned with the linear combination of the following bases

$$\left\{ \begin{pmatrix} 1 \\ 0 \\ 0 \\ 0 \end{pmatrix}, \begin{pmatrix} 0 \\ 1 \\ 0 \\ 0 \end{pmatrix}, \begin{pmatrix} 0 \\ 0 \\ 1 \\ 0 \end{pmatrix}, \begin{pmatrix} 0 \\ 0 \\ 0 \\ 1 \end{pmatrix} \right\}. \quad (9)$$

Clearly, the center of mass of this system is no longer 0 and is subject to control effort of the input signal. This finding provides us with promising intuition into locomotion planning of such robot; that is, if we can properly manipulate the frictional forces as well as the equivalent spring force inputs, the robot can produce desirable locomotion.

## B. Model simulation and result

In this subsection, we demonstrate the simulated locomotion of our robot with a selected set of inputs determined through iteration. The frictional force defined in (7) is a function of the kinetic coefficient of friction and normal force between the contacting surfaces. Here, the design, fabrication and control of the robot are highly integrated. The friction regulation method will affect all three aspects of the robot and needs to be determined in advance. Varying the normal force can be achieved by varying the mass of each block and changing the contacting surface materials will lead to switching of the coefficients of friction. While the former requires additional mechanism and reservoir to translate and store extra mass, the latter can avoid all those complications and be accomplished with an elegant design that exploits the deformation of soft materials during actuation. Additionally,

since the coefficient of kinetic friction varies between a wide range of values (0.04 for Teflon on steel and 0.8 for rubber on concrete) [28], large magnitude changes of frictional force can potentially be realized rapidly. Thus, we choose altering the contacting surfaces as the means of altering frictional force throughout the development process of our robot.

Following the described friction implementation and system dynamics discussed in Subsection III-A, we simulate the robot's dynamics as illustrated in Fig. 3. The simulation is carried out at a sampling rate of 1000 Hz to remain consistent with ensuing experiment.  $G(z)$  is the discrete-time (DT) transfer function associated with state space representation  $\begin{bmatrix} A_d & B_d^* \\ C_d & D_d \end{bmatrix}$ , of which all entries are matrices in (3) discretized using *zero-order hold* (ZOH). Similarly, all inputs and outputs here are of DT form.

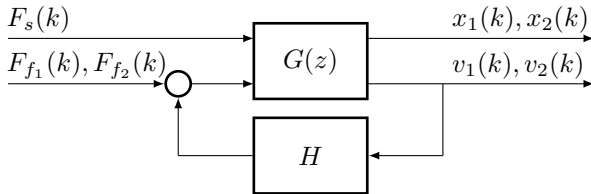


Fig. 3.  $G(z)$  is the discretized MIMO system,  $H$  is a sign operator that ensures opposing sign between  $v_1(k)$  and  $F_{f_1}(k)$ , as well as between  $v_2(k)$  and  $F_{f_2}(k)$ . Zero initial condition is selected for the simulation.

Considering the periodic contraction and elongation of the longitudinal actuator, a sinusoidal signal with amplitude and bias prescribed by forces corresponding to the minimum and maximum internal pressure is chosen to model input  $F_s$ . The pressure values are determined based off the findings in [16] and our design parameters  $F_{f_1}$  and  $F_{f_2}$  are modeled as square signals with amplitude and bias characterized by the lower and upper bounds of the kinetic frictional force corresponding to the low and high coefficients of friction, respectively. To account for the slow actuation speed of pneumatic actuators, we limit the frequency of all inputs to less than 1 Hz.  $F_{f_1}$  and  $F_{f_2}$  are set to have the same frequency but set apart with a phase differential  $\phi$  varying between 0 and  $2\pi$ . Additionally, since the kinetic friction is of opposite direction to the motion, a sign reversal operator  $H$  is introduced to ensure opposing signs between velocities and frictional forces at all times. The simulation results are presented in Fig. 4. Fig 4-(a) shows the displacements and velocities of two mass blocks when  $F_s$ ,  $F_{f_1}$  and  $F_{f_2}$  are oscillating at the frequency of 1 Hz and  $\phi$  adopts the value  $0.4\pi$ . Both masses travel approximately in a linear motion and an average speed of 6.31 m/min is derived from the displacement plot. Fig 4-(b) presents the maximum displacement traveled by the robot in correlation with input frequency assignment when  $\phi$  is held constant ( $0.4\pi$ ). It appears that for this specific selection of inputs, substantial locomotion can only be attained when the input frequencies are unified with exception of a few other frequency combinations, and in general, faster inputs lead to faster locomotion. Fig 4-(c) shows the final displacement reached by the robot across all  $\phi$  while input frequencies are held the same at 1 Hz. Clearly, it suggests that  $\phi$  is decisive to locomotion generation for this particular type of inputs and direction reversal can simply be

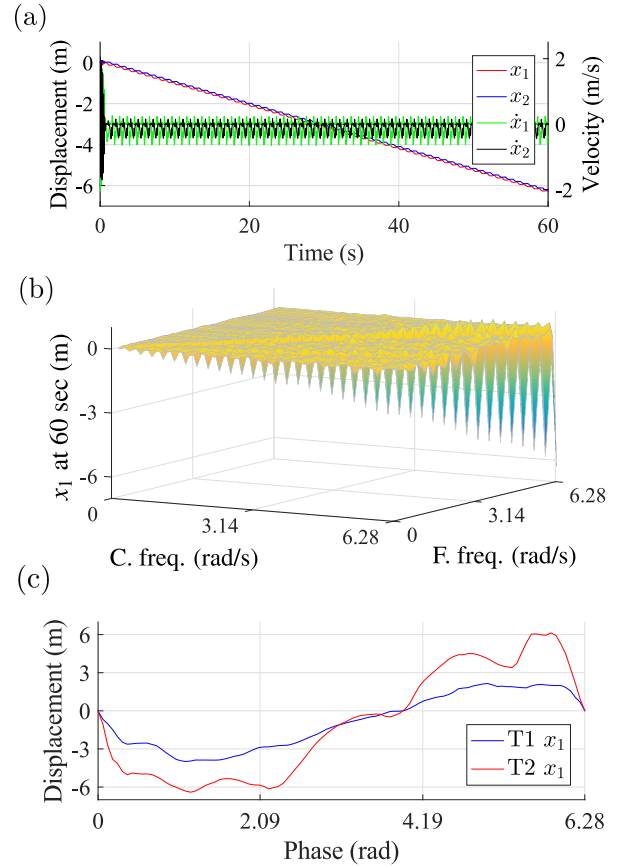


Fig. 4. (a) Displacements and velocities of  $m_1$  and  $m_2$  when the frequencies of  $F_s$ ,  $F_{f_1}$  and  $F_{f_2}$  are set to 1 Hz when  $\phi$  is  $0.4\pi$ . (b) Simulated displacement of  $m_1$  at 60 sec across a variety of combinations of  $F_s$  and  $F_{f_1}$  frequencies (unit: rad/s  $F_{f_1}$  and  $F_{f_2}$  oscillate at the same frequency and  $\phi$  is held at  $0.4\pi$ ). (c) The relationship between displacement and  $\phi$  when  $F_s$  and  $F_{f_1}$ ,  $F_{f_2}$  are synchronized (at 1 Hz). It can be observed that locomotion direction can be altered by controlling phase differential between  $F_s$  and  $F_{f_1}$ . T1, T2 represent results corresponding to mass values 0.1 and 0.2 kg, respectively. Heavier mass leads to larger friction and judging from the simulation result, larger friction results in faster locomotion.

realized by varying the phase differential between friction inputs. Such result is observed in simulations repeated for friction of different amplitudes. The findings here are limited to the inputs we have specified, but nonetheless demonstrate the great potential of generating efficient locomotion for this type of robot. A more comprehensive study on input signals and control strategies oriented to optimize locomotion is a matter of current and future research.

#### IV. DESIGN AND FABRICATION

We aim to free the existing earthworm-inspired robot [16] from its absolute reliance on environment's geometric configuration (within pipes only) to generate locomotion and enable it to crawl on surface. Therefore, the design of our robot is centered around achieving switching between different values of frictional forces between contacting surfaces. Also, since we have decided to vary the frictional force by means of changing the surfaces in contact, the design needs to incorporate multiple materials with different coefficients of friction while still being able to replicate the functional capabilities of an earthworm segment from a biologically-inspired engineering perspective. To address all these issues, we design the soft robot shown in figure Fig. 1-(c), composed

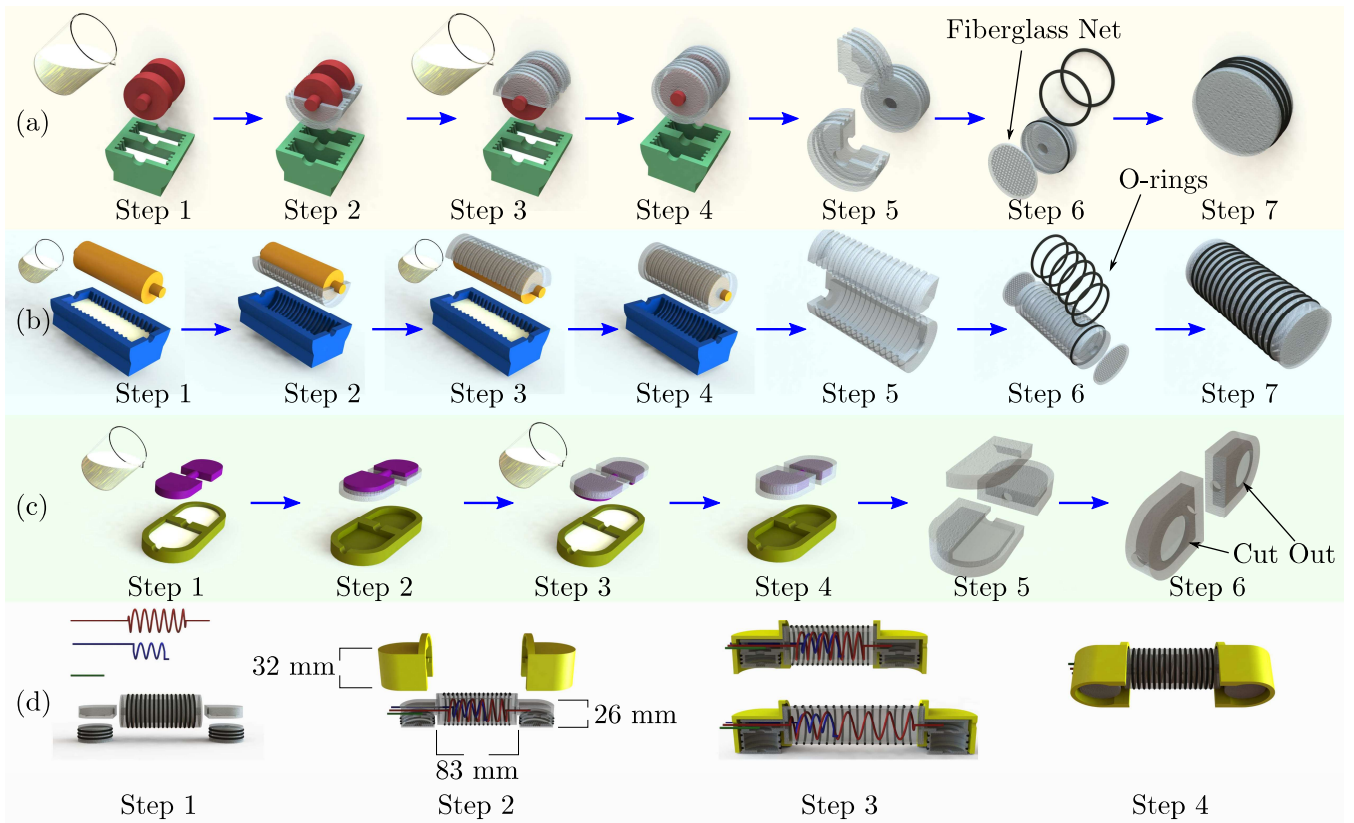


Fig. 5. **(a) Fabrication of the front and rear actuators:** First, liquid silicone (Ecoflex<sup>®</sup> 00-50, Smooth-On) is poured into the 3D-printed mold and the lower half of a symmetrical double cylindrical core is submerged in the silicone (Step 1). The silicone within the mold is then cured at 65° for 15 minutes. The cured silicone half shell together with the core it is attached to, are extracted from the mold (Step 2). Afterwards, the core is rotated 180° and liquid silicone is added into the mold again to cast the other half of the shell (Steps 3 and 4). The completed shell is then peeled off the core and Step 5 illustrates the shell's structure. In Step 6, butadiene o-rings are fitted onto the shell's imprinted grooves and a layer composed of silicone and fiberglass net is applied to seal off one end of the shell. The function of the reinforcement layer and the o-rings is consistent with that of [16]. Step 7 shows one completed front/rear actuator. **(b), (c) Fabrication of the central actuator and the connecting modules:** These use the same procedures employed in the fabrication of the front and rear actuators with the exception that the connecting modules do not require additional reinforcement layer nor o-rings. However, a hole is cut out from the bottom of both connecting modules to allow air flow into both front and rear actuators in the final assembly. **(d) Final assembly:** In Step 1, two connecting modules, a pair of front and rear actuators, a central actuator and three air feeding lines (two are helix-shaped) are integrated together. A pair of casings are then fixated over the front and rear actuator modules (Step 2). Step 3 depicts the robot in two states: when all of its actuators are either uninflated or inflated. Notice the helix structure of two air feeding lines makes possible of their simultaneous contraction and expansion with the central actuator. All sub-components are glued to each other and sealed by applying extra liquid silicone as adhesive and curing it at all conjunctions.

of three soft *artificial muscles* and two casings: a central longitudinal actuator, a pair of front and rear longitudinal actuators oriented normal to the ground, and a pair of hard casings that enclose the front and rear actuators. In addition, a pair of soft modules shown in Fig. 5-(c), are employed to connect the central actuator with the front and rear actuators. These two connecting modules are enclosed within the hard casings, as well. In the proposed robotic design, actuators are driven pneumatically. The central actuator and the pair of front and rear actuators are designed to replicate the features of earthworm's longitudinal and circular muscle, respectively. All actuators are built to expand and contract axially as functions of their internal pressures, unlike the one introduced in [16]. Both front and rear actuators are fixated to the ceilings of the hard casings and they remain above the surface without the presence of inflation as the hard casings support the robot's weight. When inflated, the front and rear actuators elongate and make contact with the surface. The hard casings provide low friction while the actuators yield high friction with the contacting surface. Here, switching

between high and low frictional force values is made possible by a simple inflation and deflation sequence. Recall from Section II, when crawling, the earthworm's relaxed circular muscles (coupled with contracted longitudinal muscles) will cause the metamere to expand radially, pushing the bristle-like setae into the ground to anchor itself to prevent backward slippage. Notice the front and rear longitudinal actuators together with their casings are inspired by earthworm's circular muscles and setae but the underlying working principles are fundamentally different. The latter utilizes hard setae to generate traction but the former employs the hard casings to reduce friction and rely on the soft actuator to increase friction. In addition, deformation of natural muscles is achieved through active contraction and passive elongation as opposed to the artificial actuators proposed here that elongate actively through inflation but contract passively.

The methods and construction sequences employed to fabricate this soft robot are depicted in Fig. 5. Fig. 5-(a), Fig. 5-(b) and Fig. 5-(c) illustrate the fabrication process of the front and rear actuators, central actuator and the connecting

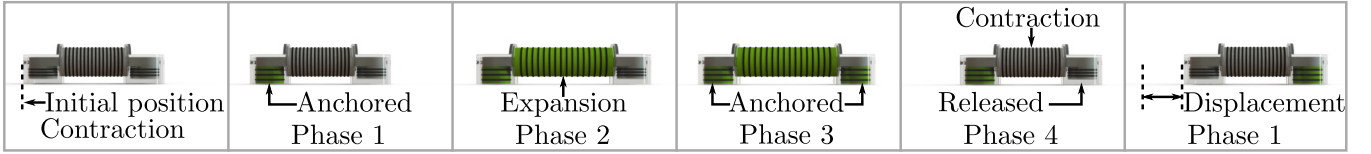


Fig. 6. When none of the actuators are inflated, both front and rear casing are in contact with the surface. In Phase 1, the rear actuator is inflated to attain contact with the surface and anchors itself. In Phase 2, the central actuator expands and drives the front actuator forward while the rear actuator remains anchored to the ground. Once central actuator stops expanding, the front actuator will inflate in Phase 3 to anchor itself to the surface. In Phase 4, both rear and central actuators contract. Such sequence is repeated to generate robot locomotion.

modules, respectively. Fig. 5-(d) chronicles the steps leading to the final assembly of the robot. The parts fabricated and materials used to build this robot include 3D-printed *acrylonitrile butadiene styrene* (ABS) molds and casings, silicone elastomer (Ecoflex<sup>®</sup> 00-50, Smooth-On), butadiene rubber elastomeric o-rings, fiberglass sheets and pneumatic components. When completed, all actuators measure 35 mm in diameter, the central actuator measures 83 mm in length and the front and rear actuator combined with the connecting modules measure 26 mm in height. The wall thickness of soft components range between 2.5 and 3 mm. These dimensions were chosen based off the robot design in [16] and modified to accommodate off-the-shelf pneumatic components.

To drive the system, an Elemental O<sub>2</sub> Commercial Air Pump and a 12-V ROB-10398 vacuum pump are employed to inflate and deflate all actuators pneumatically through a manifold (SMC VV3Q12). Three high speed solenoid valves (SMC VQ110-6M) and three Honeywell ASDX Series digital serial silicon pressure sensors are used to provide regulation and measurement of internal pressure for each actuator, respectively. All data acquisition and signal processing are realized through a data acquisition board (National Instrument PCI-6229) mounted on a target PC which communicates with a host PC via xPC Target 5.5 (P2013b).

## V. LOCOMOTION PLANNING AND CONTROL

Through our simulation results in Section III-B, We have demonstrated that substantial locomotion is contingent upon several idealized parameter approximations as well as unifying frequencies of the equivalent spring force oscillation and frictional forces switching. These conditions are either difficult to realize or not necessarily valid for the robot worm we created in Section IV. Thus replicating the simulated locomotion on the actual robot is at this moment, not a realistic objective. Here, we adopt a biologically-inspired actuation sequence to enable our robot to generate crawling motion. Notice in Fig. 2,  $m_1$  can be anchored to the ground when  $m_2$  slides forward as the central actuator elongates if

$$|F_{f_1}| \geq |F_{f_2} + F_s|. \quad (10)$$

$F_{f_1}$  is characterized as static friction here while  $F_{f_2}$  is still considered kinetic friction. And similarly,  $m_2$  can be anchored to the ground when  $m_1$  slides forward as the central actuator contracts if

$$|F_{f_2}| \geq |F_{f_1} + F_s|. \quad (11)$$

Therefore, a four-phase actuation sequence is designed to generate one complete stride sequence for our robot as

demonstrated in Fig. 6. An actuator characterization is carried out first to determine a proper set of values for the robot's *stride length*, *stance time* and *protrusion time*.

To characterize each actuator in the closed loop, three *proportional-integral-derivative* (PID) controllers  $\hat{K}_i$ , presented in Fig 7, are implemented to provide precise internal pressure regulation. During actuation, both pumps are kept operating at constant flow rate and output pressure, therefore the inflation and deflation is achieved through the rapid opening and closing of the solenoid valves which are driven by *pulse-width modulation* (PWM). The valves are normally closed, during which the manifold allows the vacuum pump to deflate. The PWM duty cycle excites valves to open and allow each actuator to inflate. The output of  $\hat{K}_i$  is the duty cycle input to each valve. Every PID controller is tuned online in an exhaustive manner.

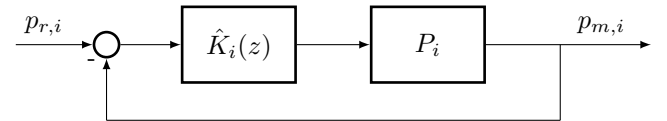


Fig. 7.  $p_{r,i}$  is the reference pressure.  $\hat{K}_i$  is PID controller tuned exhaustively for each actuator.  $P_i$  represents each valve and pressure sensor, the input to which is the duty cycle and the output is measured pressure  $p_{m,i}$ . The *root mean square error* (RMSE) of the control scheme for each actuator is limited within 0.02 psi.

The actual characterization process follows the procedure adopted in [16]. For the central actuator, a range of pressure values that lead to substantial elongation without causing significant radial expansion is identified. For the front and rear actuators, the minimum pressure threshold upon which firm contact between both actuators and surface is established is chosen to be the reference pressure. Additionally, two 130 g machined steel plates are fixed onto the top of both casings as shown in Fig.1-(c), for the purpose of increasing frictional force as well as damping the vibration caused by the rapid opening and closing of the solenoid valves during actuation. Table I summarizes a set of reference pressure values for individual actuator during each one of the four phases described in Fig. 6. The locomotion of the robot is carried out by controlling each actuator to track the reference pressure during each phase. Referring to the earthworm crawling kinematics described in Section II, we define the *protrusion time* of our proposed robot as the period during which the central actuator expands (phase 2). Similarly, the *stance time* is defined to be time duration after *protrusion time*, during which the front actuator remains static horizontally and completes a cycle of inflation and deflation (phase 3 + phase 4 + phase 1). *Protrusion time* and *stance time* are prescribed in experiments.

To implement the described locomotion method, low-level

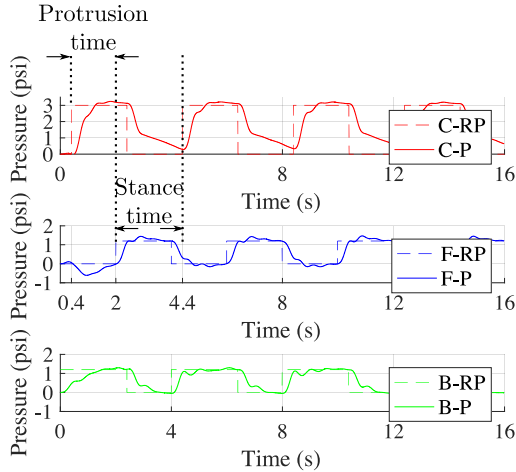


Fig. 8. Sample pressure tracking results under PID control scheme for central, front and rear actuator during locomotion. The *protrusion time* is 1.6 sec, the *stance time* is 2.4 sec and the stride period is 4 sec.

controllers composed of PIDs (Fig. 7) tuned during the characterization process are adopted to regulate the actuation of each actuator.

TABLE I  
REFERENCE PRESSURE FOR EACH ACTUATOR DURING ACTUATION

Internal Pressure (psi)	1	2	3	4
Back Actuator	1.2	1.2	1.2	0
Central Actuator	0	3	3	0
Frontal Actuator	0	0	1.2	1.2

## VI. EXPERIMENTAL RESULTS AND DISCUSSION

Experiments are carried out to validate the locomotion sequence proposed in Section V. The first set of tests is aimed to optimize the crawling speed of the robot on a single uniform surface. The influence of different variables, including the duration of each phase and reference pressures for each actuator, is examined across a broad spectrum of values. Fig. 8 presents pressure tracking of each actuator for the test that produced the fastest locomotion, in which the *protrusion time* and *stance time* were set to be 1.6 and 2.4 sec, respectively, and the reference pressures listed in Table I were adopted. A stride length of 2.79 cm and an average speed of 41.9 cm/min are observed and documented in Fig. 9. The front and rear actuator were able to track the reference pressures with minor overshoots, however, the central actuator was not able to deflate completely according to Fig. 8. Lower central actuator reference pressures and longer protrusion times were verified to produce better pressure tracking at the cost of overall locomotion speed. No obvious slippage was observed at either front and rear actuator in all tests conducted.

The second set of tests is designed to validate that our robot can travel on surface with a variety of coefficients of friction. Using the same actuation sequence, we successfully proved that the robot is able to generate peristaltic locomotion on surfaces including lab benchtop, plywood, high-density polyethylene (HDPE), aluminum plate and foam pad. Furthermore, we showed that our robot is capable of traversing surfaces of different coefficients of friction by letting it crawl from a foam pad to an HDPE

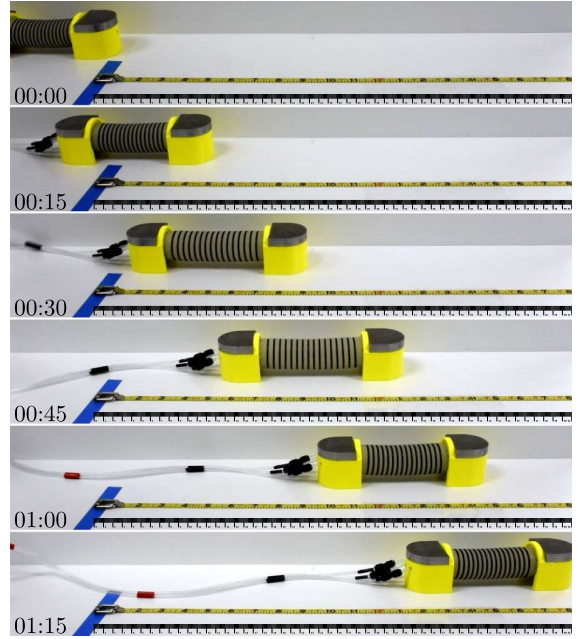


Fig. 9. Robot crawling on lab benchtop following reference pressures listed in Table I. A total distance of 52.4 cm is covered within 75 sec at an average speed of 41.9 cm/min in this test. The complete series of all experiments conducted can be found in the supporting movie S1.mp4, also available at <http://www.uscamsl.com/resources/ROBIO2017/S1.mp4>.

plate. The complete series of all the described tests can be found in the supporting movie S1.mp4, also available at <http://www.uscamsl.com/resources/ROBIO2017/S1.mp4>.

The experiments proved friction manipulation to be an efficient way to generate peristaltic crawling motion for the proposed robot. In the experiments, pressure sensors provide feedback to regulate the elongation of each actuator, therefore displacement control was only fulfilled indirectly. Direct displacement control can be implemented in the future by employing a motion capture system or soft sensors drawing inspiration from [29]. In addition, primitive actuator characterization in this work is performed empirically. An analytical model that can capture the nonlinear relationship between actuator internal pressure and deformation is needed to improve control strategy and optimize locomotion.

## VII. CONCLUSION AND FUTURE WORK

We presented an earthworm-inspired soft crawling robot capable of locomoting on surfaces by manipulating friction. The robot consists of modular actuators and casings that mimic earthworm's longitudinal and circular muscle as well as bristle-like setae structure embedded in each segment. We modeled the robot as a mass-spring system and described its crawling dynamics as an LTI system. Using the defined model, we proved that frictional force can be employed as an input that leads to system controllability. The conclusion was tested and validated through simulations. Experimentally, we demonstrated that our robot is capable of locomoting on surfaces with different coefficients of friction, emulating earthworm's peristaltic crawling.

The highly modular structure of the robot makes it easily multipliable, which leaves great potential for creating longer and more versatile robotic structures. Such complex mod-

ular system will provide an ideal platform to develop and test novel distributed control strategies. In this work, we empirically explored the feasibility of friction-manipulation generated locomotion on surfaces only. We anticipate future research will further polish the proposed robotic concept, employing only soft materials and enabling steering and locomotion on uneven terrain. Furthermore, the robot presented here is tethered to both the power source and the control feedback module, thus the overall mobility and application are highly restricted. To achieve robot autonomy, novel sensing and wireless communications need to be properly implemented. In addition, adopting portable energy resource employing methods including electrolysis [30] and combustion [31] is another focus of future research.

#### REFERENCES

- [1] D. Sadava, D. H. Hillis, H. C. Heller, and M. R. Berenbaum, *Life: The Science of Biology, 9th Edition*. Sunderland, MA: Sinauer Associates Inc., 2011.
- [2] J. B. Reece, L. A. Urry, M. L. Cain, S. A. Wasserman, P. V. Minorski, and R. B. Jackson, *Campbell Biology, 10th Edition*. Glenview, IL: Pearson, 2014.
- [3] C. A. Edwards and J. R. Lofty, *Biology of Earthworms*. London: Chapman and Hall, 2011.
- [4] K. J. Quilin, "Kinematic scaling of locomotion by hydrostatic animals: Ontogeny of peristaltic crawling by the earthworm *lumbicus terrestris*," *J. Exp. Bio.*, vol. 202, no. 6, pp. 661–674, Mar. 1999.
- [5] J. Stephenson, *The Oligochaeta*. Oxford: Clarendon Press, 1930.
- [6] S. Seok, C. D. Onal, K. Cho, R. J. Wood, D. Rus, and S. Kim, "Meshworm: A peristaltic soft robot with antagonistic nickel titanium coil actuators," *IEEE/ASME Trans. Mechatron.*, vol. 18, no. 5, pp. 1485–1497, Jun. 2006.
- [7] T. Saito, T. Kagiwada, and H. Harada, "Development of an earthworm robot with shape memory alloy and braided tube," *Adv. Robot.*, vol. 23, no. 12-13, pp. 1743–1760, 2009.
- [8] B. Kim, M. G. Lee, P. Lee, Y. Kim, and G. Lee, "An earthworm-like micro robot using shape memory alloy actuator," *Sensors Actuat. A: Phys.*, vol. 125, no. 2, pp. 429–437, Jan. 2006.
- [9] N. Saga and T. Nakamura, "Development of a peristaltic crawling robot using magnetic fluid on the basis of the locomotion mechanism of the earthworm," *Smart mater. Struct.*, vol. 13, no. 3, pp. 566–569, May. 2004.
- [10] T. Nakamura, T. Kato, T. Iwanaga, and Y. Muranaka, "Development of a peristaltic crawling robot based on earthworm locomotion," *Robot. Mechatron.*, vol. 18, no. 3, pp. 299–324, Jun. 2006.
- [11] J. Zuo, G. Yan, and Z. Gao, "A micro creeping robot for colonoscopy based on the earthworm," *J. Med. Eng. Technol.*, vol. 29, no. 1, pp. 1–7, Jan. 2005.
- [12] K. Wang, G. Yan, G. Ma, and D. Ye, "An earthworm-like robotic endoscope system for human intestine: Design, analysis, and experiment," *Ann. Biomed. Eng.*, vol. 37, no. 1, pp. 210–221, Jun. 2009.
- [13] R. F. Shepherd, F. Ilievski, W. Choi, S. A. Morin, A. A. Stokes, A. D. Mazzeo, X. Chen, M. Wang, and G. M. Whitesides, "Multigait soft robot," *Proc. Nat. Acad. Sci.*, vol. 108, no. 51, pp. 20 400–20 403, Dec. 2011.
- [14] J. K. Paik, R. K. Kramer, and R. J. Wood, "Stretchable circuits and sensors for robotic origami," in *Proc. 2011 IEEE/RSJ Int. Conf. Intell. Robots and Syst. (IROS 2011)*, San Francisco, CA, Sep. 2011, pp. 414–420.
- [15] C. Majidi, "Soft robotics: A perspective-current trends and prospects for the future," *Soft Robot.*, vol. 1, no. 1, pp. 5–11, Jul. 2013.
- [16] A. A. Calderón, J. C. Ugalde, J. C. Zagal, and N. O. Pérez-Arancibia, "Design, fabrication and control of a multi-material-multi-actuator soft robot inspired by burrowing worms," in *Proc. 2016 IEEE Int. Conf. Robot. and Biomimetics (ROBIO)*, Qingdao, China, Dec. 2016, pp. 31–38.
- [17] K. Autumn, A. Dittmore, D. Santos, M. Spenko, and M. R. Cutkosky, "Frictional adhesion: a new angle on gecko attachment," *J. Exp. Bio.*, vol. 209, no. 18, pp. 3569–3579, Aug. 2006.
- [18] A. T. Asbeck, S. Kim, M. R. Cutkosky, W. R. Provancher, and M. Lanzetta, "Scaling hard vertical surfaces with compliant microspine arrays," *Int. J. Robot. Research*, vol. 25, no. 12, pp. 1165–1179, 2006.
- [19] A. Mensiassi, D. Accoto, S. Gorini, and P. Dario, "Development of a biomimetic miniature robotic crawler," *Auton. Robots*, vol. 21, no. 2, pp. 155–163, 2006.
- [20] J. Koh and K. Cho, "Omega-shaped inchworm-inspired crawling robot with large-index-and-pitch (lip) sma spring actuators," *IEEE/ASME Trans. Mechatronics*, vol. 18, no. 2, pp. 419–429, Apr. 2013.
- [21] M. Schulke, L. Hartmann, and C. Behn, "Worm-like locomotion systems: Development of drives and selective anisotropic friction structures," in *Proc. 56th Int. Scientific Colloq.*, Ilmenau, Germany, Sep. 2011.
- [22] V. Vikas, E. Cohen, R. G. adn C. Sözer, and B. Trimmer, "Design and locomotion control of soft robot using friction manipulation and motor-tendon actuation," *IEEE Trans. Robot.*, vol. 32, no. 4, pp. 949–959, May 2016.
- [23] C. Darwin, *The formation of vegetable mould, through the action of worms, with observations on their habits*. London: John Murray, 1881.
- [24] T. Noritsugu and M. Kubota, "Development of in-pipe mobile robot using pneumatic soft-actuator," *J. Robot. Soc. Japan*, vol. 18, no. 6, pp. 831–838, Aug. 2000.
- [25] C. Chen, *Linear System Theory and Design, 4th Edition*. New York, NY: Oxford University Press, 2013.
- [26] G. E. Dullerud and F. Paganini, *A Course in Robust Control Theory A Convex Approach*. New York, NY: Springer, 2013, vol. 36.
- [27] E. Berger, "Friction modeling for dynamic system simulation," *Appl. Mechanics Rev.*, vol. 55, no. 6, pp. 535–577, 2002.
- [28] H. D. Young, R. A. Freedman, and L. Ford, *University Physics with Modern Physics, 12th Edition*. Boston, MA: Addison-Wesley, 2007.
- [29] Y. Park, B. Chen, and R. J. Wood, "Design and fabrication of soft artificial skin using embedded microchannels and liquid conductors," *IEEE Sensor J.*, vol. 12, no. 8, pp. 2711–2718, 2012.
- [30] H. Gensler, R. Sheybani, P. Li, R. Lo, and E. Meng, "An implantable mems micropump system for drug delivery in small animals," *Biomed. Microdevices*, vol. 14, no. 3, pp. 483–496, Jun. 2012.
- [31] R. F. Shepherd, A. A. Stokes, J. Freake, J. Barber, P. W. Snyder, A. D. Mazzeo, L. Cademartiri, S. A. Morin, and G. M. Whitesides, "Using combustion to power a soft robot," *Angew. Chem. Int. Ed.*, vol. 52, no. 10, pp. 2892–2896, Mar. 2013.